

Phosphotungstic anion-paired quinoline salt for heterogeneous photocatalytic hydroxylation of benzene to phenol with air

Lingyu Zhang¹, Qian Hou¹, Yu Zhou^{*}, Jun Wang^{*}

State Key Laboratory of Materials-Oriented Chemical Engineering, College of Chemical Engineering, Nanjing Tech University, Nanjing, 210009, China

ARTICLE INFO

Keywords:

Photocatalysis
Ionic liquids
Polyoxometalates
Heterogeneous catalysts
Benzene hydroxylation to phenol

ABSTRACT

Heterogeneous catalysts are preferred in production of chemicals due to the facile production separation and catalyst reuse. However, it is still one challenge to construct efficient heterogeneous catalyst for target reaction. Herein, functional polyoxometalates paired ionic salts (IL-POMs) were prepared through pairing quinoline cations with Keggin-type phosphotungstic (PW) anions. Long alkyl chain in the organic cations enabled the solid nature of these hybrids and endowed them as the recyclable heterogeneous photocatalysts. They exhibited high yield (20.9%) and selectivity (> 99%) in the benzene hydroxylation to phenol by using atmospheric air as the sole oxidant. The activity of the IL-POM hybrid is even higher than the quinoline salt precursor, thanks to the unique redox property of PW anions that promotes the generation, separation and transport of photo-induced carriers. After reaction, the catalyst was facilely reused with stable activity. The catalyst was also active and recoverable in the oxidation of benzyl alcohol to benzaldehyde with atmospheric air.

1. Introduction

Environment and energy problems are two of the crucial bottlenecks that restrict the sustainable development, urgently encouraging the search of clean, atom economy and environmentally friendly route to produce fine chemicals [1–3]. Unfortunately, many important bulk chemicals are still produced through traditional energy-consuming and polluted pathways [3,4]. It is exemplified by the production of phenol, one of the most valuable intermediates with wide applications such as the precursors of resins, dyes, pharmaceuticals, and agrochemicals [5–7]. Currently, the majority of phenol is industrially produced via a three-step cumene process with many deficiencies such as low yield, high energy consumption, harsh reaction conditions and the formation of equimolar amounts of acetone as the byproduct [8–11]. One attractive alternative is the direct oxidation of benzene to phenol with green oxidants such as hydrogen peroxides (H₂O₂) and molecular dioxygen (O₂) [12–15]. However, product phenol is more active than the inert substrate benzene, making this selective oxidation great challengeable [14,16,17]. As a result, great efforts have been devoted to the photocatalytic benzene hydroxylation to phenol through driving the chemical transformation with the aid of light energy [18].

Various homogeneous and heterogeneous photocatalysts have been explored in the photocatalytic oxidation of benzene to phenol [19–22].

The utilization of H₂O₂ as the terminal oxidant was extensively studied, but the oxidation of benzene with the low cost and easily available O₂ is still scarce [22], attributable to that both benzene and O₂ are inert reactants. Up to now, several supported noble metal nanoparticles and organic molecules were applied to the photocatalytic conversion of benzene to phenol with O₂ either under UV or visible light irradiation, with their recycling performance unknown [23–27]. Recently, using Bi₂WO₆/CdWO₄ hybrid as a photocatalyst and O₂ as the oxidant afforded a phenol yield of 7.3% and no apparent deactivation was observed in the recycling test [28]. Thereupon, it is exceedingly requireable but still challengeable to design highly efficient heterogeneous recyclable photocatalyst for the oxidation of benzene to phenol with O₂.

Organic molecules with extended conjugated structure such as aromatic ketones/quinones, heterocycles and dyes are efficient and versatile photoactive sites via the formation of the highly reactive intermediate under mild conditions [26,27,29–31]. They have almost unlimited structure and their functionality can be task-specifically designed at molecular level [29]. However, this kind of photocatalysts is normally soluble in common solvents, which is disadvantageous for their recovery and recycling utilization. Ionic liquids (ILs) and their derivatives are organic ionic salts and have also applied in the homogeneous and heterogeneous photocatalytic systems [26,32,33]. The artificial structure of ILs endows them great designability and wide

^{*} Corresponding authors.

E-mail addresses: njtzhouyu@njtech.edu.cn (Y. Zhou), junwang@njtech.edu.cn (J. Wang).

¹ These two authors contributed equally: Lingyu Zhang and Qian Hou.

potential applicability, as special organic molecular catalysts [34]. More importantly, compared with the neutral organic molecules, the solubility of ILs is facilely modulated by varying the cations and anions [35,36]. Solidification of ILs have been reached by pairing organic ionic cations with polyoxometalate (POM) anions, the transition-metal oxo-anion clusters with versatile adjustable structure plus versatile acid/base and redox catalytic properties [35]. The unique properties above promote the development of various POMs as efficient homogeneous catalysts in numerous acids, bases and oxidation reactions [35–38,40,41]. However, the dissolution of POMs in many polar solvents increases the difficulties in the recovery, separation, and recycling of the catalysts [35], just like the situation of organic molecules. Up to now, both quinolinium ions, a kind organic molecule [26], and POM species [37,41] have been applied in the photocatalytic benzene hydroxylation to phenol, yet, no organic molecule or POM related heterogeneous catalysts have been constructed for this process. Combination of organic cations and POM anions offered a series of POM-based ionic salts (shorten as IL-POMs) as efficient heterogeneous catalysts in many organic reactions [37–40]. It is proposed that IL-POMs would include the character and catalytic properties of organic molecules and POM species in one catalyst [35,36,39,40], and more importantly, enable a facile strategy towards heterogeneous catalysts. Besides, owing to the existence of strong electrostatic interaction between the cations and anions, the photochemistry properties of IL-POMs would be modulated through task-specially designing the organic cations and POM anions. However, to the best of our knowledge, the application of IL-POMs in heterogeneous photocatalysis is to be explored.

In this work, a series of IL-POM hybrids were constructed by pairing quinoline cations with phosphotungstic (PW) anions and their photocatalytic performance in benzene hydroxylation to phenol with air was investigated. We demonstrate that the length of the carbon chain in the alkyl groups of quinoline cations is crucial for the solubility of these IL-POMs and long carbon chain led to the formation of heterogeneous photocatalysts. The obtained IL-POM exhibited high photocatalytic activity in the benzene hydroxylation to phenol by using air as the sole oxidant. After reaction, the catalyst was facilely recovered and reused with excellent recyclability. Based on the full characterization and control experiments, a synergistic effect between IL cations and POM anions is proposed to understand the reaction. Further, their application in heterogeneous photocatalytic oxidation of benzyl alcohol to benzaldehyde with air was also explored to reveal the rationality of the structural design of this photocatalyst.

2. Experimental section

2.1. Materials and methods

All the commercial chemicals were analytical grade and used as received. The CHN elemental analysis was performed on an elemental analyzer Vario EL cube. Thermo gravimetry (TG) analysis was carried out on a STA409 instrument (dry air, $10\text{ }^{\circ}\text{C min}^{-1}$). Scanning electron microscopy (SEM) images and energy-dispersive X-ray spectrometry (EDS) elemental mapping analysis was recorded on a HITACHI S-4800 field-emission scanning electron microscope. Transmission electron microscopy (TEM) images were collected on a jeol 2100 plus field-emission transmission electron microscope. ^1H nuclear magnetic resonance (NMR) spectra were collected on a Bruker DPX 500 spectrometer at ambient temperature by using dimethyl sulfoxide (DMSO) as the solvent and tetramethylsilane (TMS) as the internal reference. Solid state ^{13}C and ^{31}P magic angle spinning (MAS) NMR spectra were recorded on a Bruker AVANCE-III spectrometer (9.4 T, 100 MHz for ^{13}C nuclei and 161.996 MHz for ^{31}P nuclei with a CP/MAS unit). X-ray diffraction (XRD) patterns ranging $5\text{--}80^{\circ}$ ($0.2^{\circ}\text{ s}^{-1}$) were recorded using a SmartLab diffractometer from Rigaku equipped with a 9 kW rotating anode Cu source (40 kV, 20 mA). N_2 sorption isotherms were measured at 77 K using a BELSORP-MINI analyzer. Before measurement, the

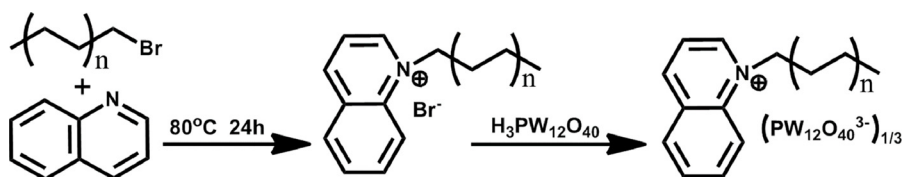
samples were degassed at $100\text{ }^{\circ}\text{C}$ for 3 h. X-ray photoelectron spectroscopy (XPS) was performed on a PHI 5000 Versa Probe X-ray photoelectron spectrometer equipped with Al K α radiation (1486.6 eV). Photoluminescence (PL) spectra were collected on a Varian Cary Eclipse spectrophotometer. Attenuated total reflection-Fourier transform infrared spectra (ATR-FTIR) were measured on an Agilent Cary 660 instrument in the region $4000\text{--}400\text{ cm}^{-1}$. Solid UV-vis spectra were recorded on a SHI-MADZU UV-2600 spectrometer with barium sulfate (BaSO_4) as an internal standard. Electron spin-resonance (ESR) spectra were measured with a Bruker EMX-10/12 spectrometer at the X-band. Liquid chromatography-tandem mass spectrometry (LC-MS/MS) was recorded by using an Agilent 1260 LC system equipped with an EC-C18 column and equilibrated with 90% solvent A (water) and 10% solvent B (methanol) for the chromatographic separation. An Agilent Technologies 6540 UHD quadrupole time-of-flight (Q-TOF) mass spectrometer was used for the MS/MS analysis and operated in positive electrospray ionization (ESI) mode. Photoelectrochemical properties were analyzed by using a CHI 760E electrochemical station (Shanghai Chen-hua, China) by using a conventional three electrode configurations with Pt foil and Ag/AgCl (saturated KCl) as the counter electrode and reference electrode, respectively. The working electrodes were prepared by depositing the photocatalyst ink on glassy carbon. The catalyst (2.0 mg) was dispersed in a mixture solution of ethanol (1 mL) and nafion (100 μL) and then sonicated for 30 min. The resulting catalyst ink (20 μL) was dropwise deposited onto glassy carbon electrode ($\varphi=6\text{ mm}$). Photocurrent measurement and electrochemical impedance spectroscopy (EIS) were measured at open circuit potential by using 0.1 M Na_2SO_4 aqueous solution as the electrolyte.

2.2. Synthesis of IL-POM

IL-POM hybrids were prepared with a two-step synthetic method. The following is the detailed synthesis of the typical sample $\text{C}_{16}\text{Qu-PW}$. Cetylquinolinium bromide ($\text{C}_{16}\text{Qu-Br}$) was synthesized by referring to our previous report [34]. Quinoline (20 mmol) and 1-bromohexadecane (10 mmol) were mixed in a 25 mL round-bottomed flask and then stirred at $80\text{ }^{\circ}\text{C}$ for 24 h. After reaction, the precipitate was isolated by filtration, washed with ethyl acetate, and then dried to afford $\text{C}_{16}\text{Qu-Br}$ as a red solid. Elemental analysis (Table S1) calcd (wt%): C 69.11, H 3.22, N 9.28; found (wt %): C 69.16, H 3.13, N 9.17. ^1H NMR (500 MHz, $\text{D}_6\text{-DMSO}$, TMS) (Fig. S1) δ (ppm) = 0.86 (t, 3H, $-\text{CH}_3$), 1.28 (m, 24H, $-\text{CH}_2$), 1.41 (t, 2H, $-\text{CH}_2$), 1.98 (t, 2H, $-\text{CH}_2$), 5.10 (t, 2H, $-\text{CH}_2$), 8.08 (t, 1H, $-\text{CH}$), 8.23 (t, 1H, $-\text{CH}$), 8.31 (t, 1H, $-\text{CH}$), 8.54 (d, 1H, $-\text{CH}$), 8.67 (d, 1H, $-\text{CH}$), 9.34 (d, 1H, $-\text{CH}$), 9.64 (d, 1H, $-\text{CH}$). The catalyst $\text{C}_{16}\text{Qu-PW}$ was synthesized through the reaction of $\text{C}_{16}\text{Qu-Br}$ and phosphotungstic acid (H_3PW). A solution of H_3PW (0.25 mmol H_3PW in 30 mL ethanol) was dropwise added into the solution of $\text{C}_{16}\text{Qu-Br}$ (0.75 mmol $\text{C}_{16}\text{Qu-Br}$ in 30 mL ethanol). The mixture was stirred at room temperature for 24 h. The formed pink precipitate $\text{C}_{16}\text{Qu-PW}$ was isolated by filtration, washed with ethanol and then dried under the vacuum. Elemental analysis (Table S1) calcd (wt %): C 22.86, H 3.07, N 1.07; found (wt %) C 23.03, H 3.16, N 1.03. $^1\text{HNMR}$ (500 MHz, $\text{D}_6\text{-DMSO}$, TMS) (Fig. S2) δ (ppm) = 0.85 (t, 3H, $-\text{CH}_3$), 1.23 (m, 24H, $-\text{CH}_2$), 1.43 (t, 2H, $-\text{CH}_2$), 2.01 (t, 2H, $-\text{CH}_2$), 5.09 (t, 2H, $-\text{CH}_2$), 8.08 (t, 1H, $-\text{CH}$), 8.21 (t, 1H, $-\text{CH}$), 8.31 (t, 1H, $-\text{CH}$), 8.52 (d, 1H, $-\text{CH}$), 8.63 (d, 1H, $-\text{CH}$), 9.31 (d, 1H, $-\text{CH}$), 9.57 (d, 1H, $-\text{CH}$).

2.3. Catalytic activity

Photocatalytic benzene hydroxylation to phenol was carried out under ambient conditions (room temperature and atmospheric pressure). Typically, benzene (1.28 mmol), water (1 mL), catalyst (25 μmol) and acetonitrile (10 mL) were added into a 70 mL Pyrex glass bottle. The suspension was stirred for 30 min and then irradiated by a high pressure mercury lamp (500 W, $\lambda \leq 365\text{ nm}$) using a photocatalysis

Scheme 1. Preparation of $C_n\text{Qu-PW}$ hybrids.

instrument BL-GHX-V (Shanghai Bi Lang Co., LTD, China). After reaction, the liquid phase was isolated by centrifugation and analyzed by gas chromatography (GC, Agilent GC 7890B) equipped with a hydrogen flame ionization detector and a capillary column (HP-5, 30 m \times 0.25 mm \times 0.25 μm). The potential by-products such as benzoquinone and benzenediol were not detected by GC, giving the GC selectivity above 99%. Yield of phenol = $\text{mmol}(\text{phenol}) / \text{mmol}(\text{initial benzene}) \times 100\%$. Photocatalytic selective oxidation of benzyl alcohol was performed similarly. Reusability was evaluated in a six-run recycling test. After reaction, the catalyst was isolated by centrifugation, washed with ethanol and then directly charged into the next run.

3. Results and discussion

3.1. Structure characterization

IL-POM hybrids were synthesized through the reaction of phosphotungstic acid (H_3PW) and alkyl functional quinoline salts (Scheme 1). These quinoline-based ionic salts and IL-POMs are termed

$C_n\text{Qu-Br}$ and $C_n\text{Qu-PW}$ ($n = 2, 8, 12, 16$ or 18 , denoting the length of the carbon chain in the alkyl groups), respectively. Experimental CHN elemental analyses (Table S1) were matching with the molecular structure of $C_n\text{Qu-Br}$ and indicated that each $C_n\text{Qu-PW}$ molecule is composed of three $C_n\text{Qu}^+$ cations and one phosphotungstate anion ($\text{PW}_{12}\text{O}_{40}^{3-}$, shorten as PW anion). Additional characterization was performed on the typical ionic salt $C_{16}\text{Qu-Br}$ and corresponding IL-POM hybrid $C_{16}\text{Qu-PW}$. ^1H NMR spectra (Fig. S1 and S2) and liquid chromatography-tandem quadrupole time-of-flight mass spectrometry (LC-Q-TOF) analysis (Fig. S3) additionally proved the above-mentioned molecular formula of $C_{16}\text{Qu-Br}$ and $C_{16}\text{Qu-PW}$.

Fig. 1A shows the FT-IR spectra of $C_{16}\text{Qu-PW}$ and its two precursors of H_3PW and $C_{16}\text{Qu-Br}$. The IR spectrum of H_3PW displayed four characteristic vibration bands for Keggin structure, in which the bands at 1080, 983, 888 and 813 cm^{-1} are assignable to the stretching vibration of the central oxygen $\nu(\text{P-Oa})$, terminal oxygen $\nu(\text{W=Ot})$, inter-octahedral oxygen $\nu(\text{W-Ob-W})$ and intra-octahedral oxygen $\nu(\text{W-Oc-W})$, respectively [42]. The structure of Keggin-type phosphotungstic (PW) anions is supplemented in Fig. S4. The IR spectrum of $C_{16}\text{Qu-PW}$ also exhibited the peaks at 1626–1363 cm^{-1} and 2992–2850 cm^{-1} for the quinoline unit and alkyl chain, which were found in the spectrum of $C_{16}\text{Qu-Br}$ [43]. Four peaks for the Keggin structure of PW anions were still observable in the spectrum of $C_{16}\text{Qu-PW}$. The slight peak shifts suggest the strong ionic interaction between organic cations and PW anions, which accounts for the solid nature of $C_{16}\text{Qu-PW}$. This hybrid is modestly soluble in DMSO but is insoluble in most common solvents, such as water, alcohols, acetonitrile, acetone, and ethyl acetate. By contrast, samples $C_{2-12}\text{Qu-PW}$ obtained from the quinoline salts tethered with short alkyl chains were soluble in these solvents, whereas $C_{18}\text{Qu-PW}$ has the same solubility as $C_{16}\text{Qu-PW}$. This phenomenon implies that the solubility of $C_n\text{Qu-PW}$ relies on the length of the carbon chain in the organic cations. XRD patterns of H_3PW , $C_{16}\text{Qu-Br}$ and $C_{16}\text{Qu-PW}$ are shown in Fig. 1B. The neat H_3PW presents a set of sharp Bragg peaks for the secondary crystal structure. $C_{16}\text{Qu-Br}$ also exhibited crystal structure. All of these peaks didn't appear in the spectrum of $C_{16}\text{Qu-PW}$ and only a broad Bragg peak was observable at $2\theta = 8.1^\circ$ with a d spacing of 1.1 nm, close to the theoretical size of a primary unit of IL-POM hybrid [44,45]. The chemical structure of $C_{16}\text{Qu-PW}$ was further investigated by solid state NMR analyses. In the

^{13}C NMR spectrum (Fig. 1C), the peak at 138 ppm is ascribed to the C7 and C9 carbon atoms in the quinoline ring. The peak at 132 ppm is assignable to the C4-6 carbon atoms. The peaks at 151, 149, 124, and 119 ppm are respectively attributable to the C3, C1, C2, and C8 carbon atoms. The peak at 61 ppm comes from the methylene (C10) bonded directly to the nitrogen atom. The peaks at 31 and 23 ppm respond respectively to the other methylene (C11-23 and C24) in the hexadecyl line. The peak at 15 ppm is corresponding to the terminal methyl (C25) moiety of hexadecyl line. All of these ^{13}C NMR

signals additionally confirm the structure of $C_{16}\text{Qu-PW}$. ^{31}P NMR spectrum of $C_{16}\text{Qu-PW}$ (Fig. 1D) demonstrated a dissymmetry signal at -15.9 ppm. Phosphotungstic acid itself has a sharp and symmetric resonance peak at -15.2 ppm characteristic of phosphorous in the central position of the Keggin unit [46]. The asymmetrical resonance signal with slight shifting to up-field for $C_{16}\text{Qu-PW}$ is attributable to the strong interaction between organic cations and Keggin type POM anions [47].

SEM images indicated that the primary particles of $C_{16}\text{Qu-PW}$ are irregular ones with the size of hundreds of nanometers (the inset image of Fig. 2A). These primary particles are highly interconnected and fused with each other to generate secondary particles with the size from several to tens of micrometers. Elemental mapping images showed the existence of C, N, O, P and W elements, which suggested that phosphotungstic acid was exchanged successfully. TEM images further visualized the morphology information observed in the SEM images. Nitrogen sorption experiment shown the low uptake in the whole pressure range (Fig. S5), indicating that the obtained $C_{16}\text{Qu-PW}$ is of nonporous structure with the surface area below $1 \text{ m}^2 \text{ g}^{-1}$. TG curve in Fig. S6 illustrated that $C_{16}\text{Qu-PW}$ possesses a thermally stable structure with the starting decomposition temperature up to 330 $^\circ\text{C}$. The drastic weight loss ranging from 330 to 400 $^\circ\text{C}$ and the slight weight loss from 400 to 530 $^\circ\text{C}$ are assigned to the decomposition of hexadecyl group of the organic cations. The weight loss from 530 to 640 $^\circ\text{C}$ is mainly attributed to the decomposition of the quinoline group. The total weight loss of 26.9% in the range of 330-640 $^\circ\text{C}$ is consistent with the theoretical one 27.0%, further verifying the rationality of the chemical composition of this IL-POM hybrid.

The surface chemical compositions and bonding configurations of $C_{16}\text{Qu-Br}$ and $C_{16}\text{Qu-PW}$ were investigated by X-ray photoelectron spectroscopy (XPS). The C 1s, N 1s and Br 3d signals at 284.14, 401.82, 67.24 eV were observed in the survey scan spectrum of $C_{16}\text{Qu-Br}$ (Fig. S7). The high-resolution C 1s signal was fitted with three peaks at 289.33, 286.26 and 285.19 eV for the C on the alkyl chain, aromatic ring and the end of chain, respectively (Fig. S8) [48]. Only one N 1s peak was identified at 401.82 eV for quinoline nitrogen (Fig. 3A) [49]. The Br 3d spectrum was deconvoluted into two peaks at 68.44 eV and 67.50 eV, which is belonged to Br anion (Fig. 3B) [50]. The survey scan spectrum of $C_{16}\text{Qu-PW}$ exhibited the C 1s, N1s, P 2p and W 4f signals at 284.69, 401.82, 135.08 and 36.35 eV. The presence of P and W signals and the absence of Br signal indicated that the Br anions has been exchanged to be PW anions (Fig. S7). Compared with $C_{16}\text{Qu-Br}$, the C 1s signals of $C_{16}\text{Qu-PW}$ shifted to the lower binding energy. One weak P 2p signal was found at 135.08 eV (Fig. 3C), while the W 4f signal was deconvoluted into two sets of peaks (Fig. 3D). The ones at 36.66 eV (W 4f7/2) and 39.20 eV (W 4f5/2) were equal to that of W^{6+} species that are same as the PW anions of neat H_3PW . W 4f peaks at lower binding energies at 35.82 and 37.99 eV were corresponded to the W^{5+} species, the formation of which comes from the electron transfer from $C_{16}\text{Qu}$ cations to PW anions due to the strong electronic cation-anion

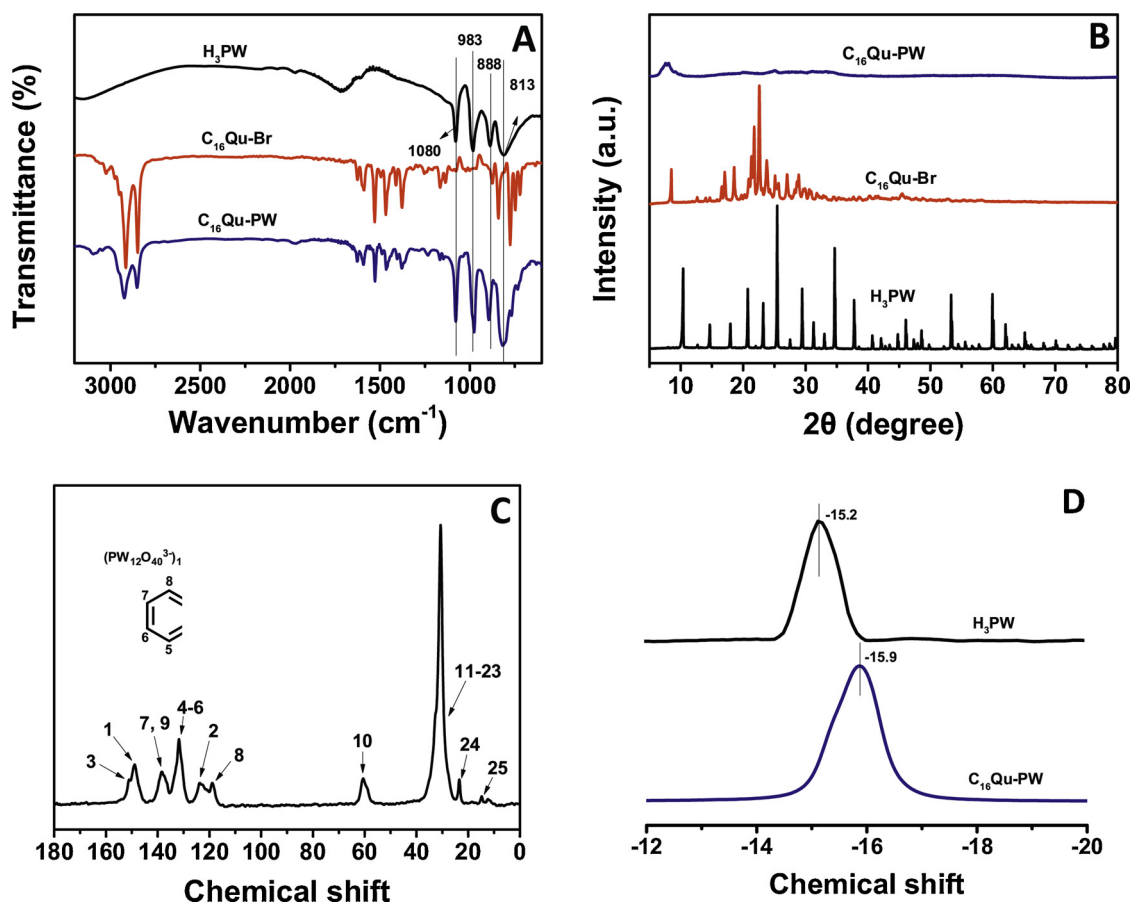


Fig. 1. (A) FT-IR spectra, (B) XRD patterns of H₃PW, C₁₆Qu-Br and C₁₆Qu-PW; (C) ¹³C and (D) ³¹P MAS NMR spectra of H₃PW and C₁₆Qu-PW.

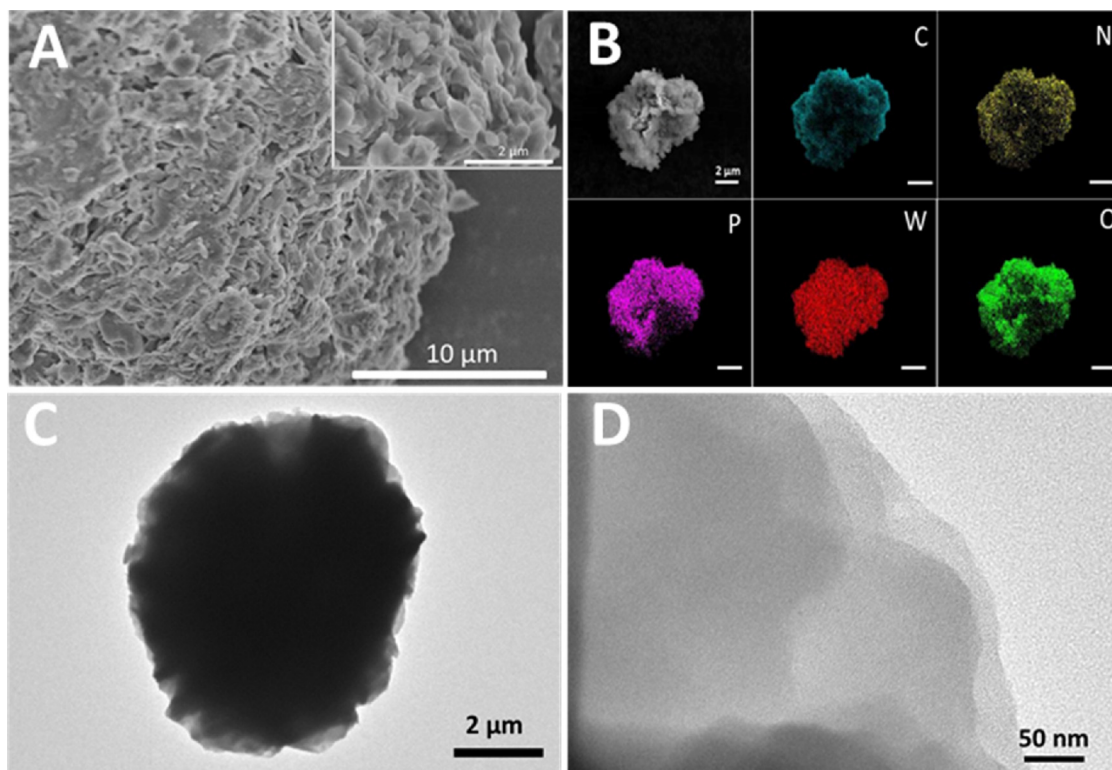


Fig. 2. (A, B) SEM and corresponding EDX mapping images for C, N, P, W, and O elements, and (C, D) TEM images of C₁₆Qu-PW.

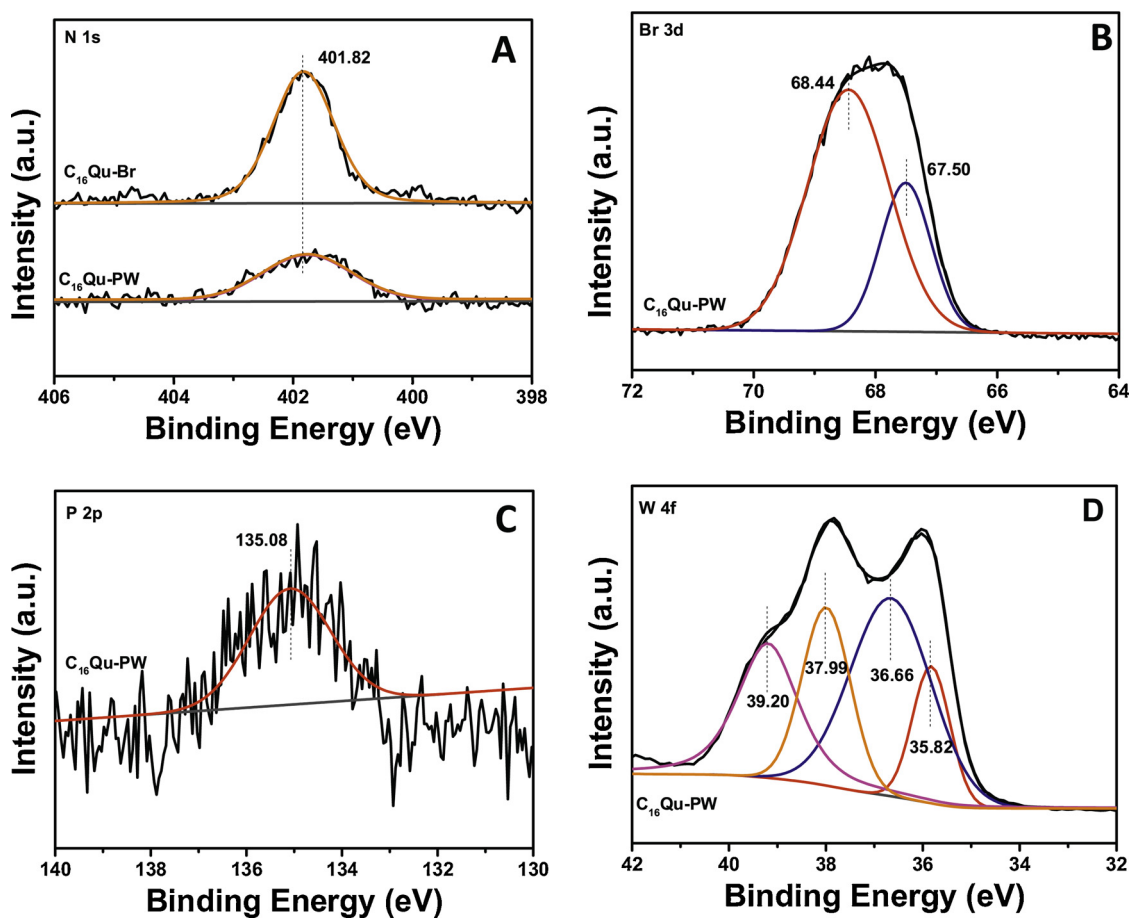


Fig. 3. High-resolution (A) N 1s, (B) Br 3d, (C) P 2p, and (D) W 4f XPS spectra.

interaction [51].

UV-vis spectra were employed to detect the optical properties of these IL-POM hybrids (Fig. 4A). H_3PW presented two strong absorption bands centered at 260 and 310 nm for the ligand to metal charge transfer (O^2-W^{6+}) in the Keggin units [52]. The absorption band centered at 320 nm and a broad peak centered at 500 nm belong to $\pi-\pi^*$ transition and $n-\pi^*$ transition of organic compound [53]. Similar UV-vis spectra of $C_{16}Qu-Br$ and $C_{16}Qu-PW$ were observed, suggesting that these adsorption bands mainly come from the organic cations [54,55]. The enhanced absorption band from 200 to 400 nm of $C_{16}Qu-PW$ is a synergistic effect of organic cations and PW anions, reaching an enhanced absorption in the UV region. The inset of Fig. 4A shown energy gaps calculated from Tauc plots, which are 2.90, 2.72 and 2.80 eV for H_3PW , $C_{16}Qu-Br$ and $C_{16}Qu-PW$ respectively. The electron behaviors and photophysical properties of $C_{16}Qu-Br$ and $C_{16}Qu-PW$ were investigated by photoluminescence (PL) emission spectra. PL emission reflects the recombination of photogenerated charge carriers, in which weaker PL intensity is generally corresponding to lower recombination rate of photogenerated electrons and holes [56]. Fig. 4B compares the PL emission spectra of $C_{16}Qu-Br$ and $C_{16}Qu-PW$. It was found that $C_{16}Qu-Br$ exhibited emission at 600 nm, indicating that electrons can be excited by $C_{16}Qu-Br$. Compared to $C_{16}Qu-Br$, the intensity of PL emission spectrum for $C_{16}Qu-PW$ showed a distinct drop off at this band [57]. This dramatic difference suggests that the recombination of photoexcited carriers is efficiently restrained after pairing $C_{16}Qu^+$ cations with PW^{3-} anions. In addition, photocurrent

measurement and electrochemical impedance spectroscopy (EIS) were carried out on $C_{16}Qu-Br$ and $C_{16}Qu-PW$. The photocurrent increases sharply upon light irradiation and returns quickly to its dark-current state when the light turns off (Fig. 4C). The dramatically

strengthened photocurrent density of $C_{16}Qu-PW$ relative to that of $C_{16}Qu-Br$ indicates that more excited electrons were generated and efficiently separated on the former [58,59]. Fig. 4D compares EIS spectra of these two samples. Only one arc/semicircle in the frequency ranges was observed in each spectrum, indicating the involvement of surface charge-transfer in the photocatalytic reaction system. The semicircle diameter of $C_{16}Qu-PW$ was much smaller than that of $C_{16}Qu-Br$, reflecting the reduced charge transfer resistance that would efficiently promote the separation of photoinduced electron-hole pairs and substantially accelerate the interfacial charge transfer [60]. All these photoelectrochemical results reveal the improved efficient in the generation, separation and transport of photoinduced carriers on $C_{16}Qu-PW$ relative to $C_{16}Qu-Br$. Ultimately, more separated photogenerated charge carriers give rise to the higher photocatalytic activity.

3.2. Photocatalytic hydroxylation of benzene to phenol

The photocatalytic performance of C_nQu-PW series and various control materials were assessed in hydroxylation of benzene to phenol using atmospheric air as the sole oxidant (Table 1). No phenol was detectable in the absent of a catalyst and only trace amount of phenol formed by using quinoline (Qu), 1-bromohexadecane ($C_{16}Br$) or Na_3PW as the homogeneous photocatalysts (Entries 1-4). The yield of phenol was 14.1% over the organic salt $C_{16}Qu-Br$, which is also soluble in the reaction mediate of mixture of acetonitrile and water (Entry 5). $C_{16}Qu-PW$ served as a heterogeneous catalyst and offered a high yield of 20.9% (Entry 6). No formation of phenol was observable when performing the $C_{16}Qu-PW$ catalyzed reaction in the dark (Entry 7), illustrating the photocatalytic nature. The higher activity of $C_{16}Qu-PW$ than $C_{16}Qu-Br$ is in line with the weaker peak intensity in the PL spectrum

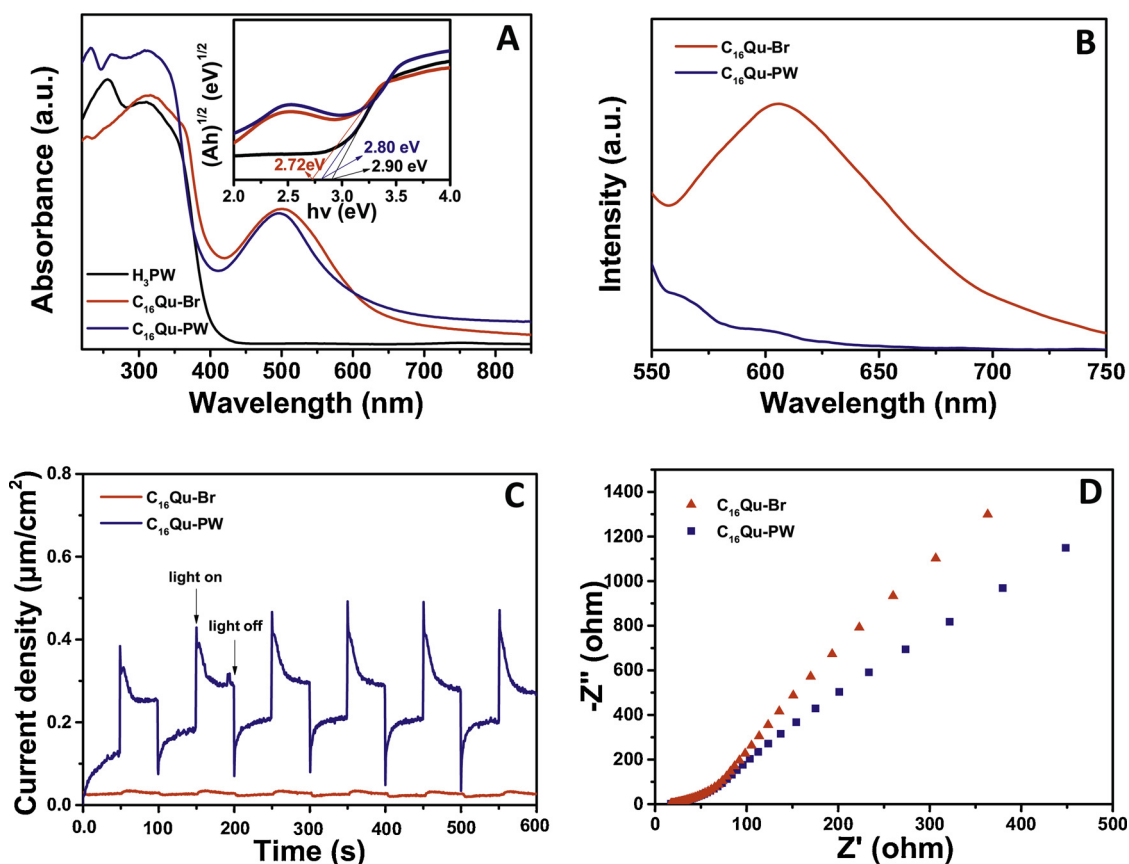


Fig. 4. (A) UV-vis spectra (the inset shows the corresponding Tauc plots) of H_3PW , $C_{16}Qu-Br$ and $C_{16}Qu-PW$; (B) PL spectra, (C) transient photocurrent response and (D) electrochemical impedance spectra of $C_{16}Qu-Br$ and $C_{16}Qu-PW$.

Table 1
Photocatalytic selective oxidation of benzene to phenol^a.

Entry	Catalyst	Catalyst dosage (μmol)	Phenomenon	Atmosphere	Yield (%)	Sel. (%)
1	None	–	–	Air	< 0.1	–
2	Qu	75	Homogeneous	Air	0.3	> 99
3	$C_{16}Br$	75	Homogeneous	Air	< 0.1	–
4	Na_3PW	25	Homogeneous	Air	< 0.1	–
5 ^b	$C_{16}Qu-Br$	75	Homogeneous	Air	14.1	> 99
6	$C_{16}Qu-PW$	25	Heterogeneous	Air	20.9	> 99
7 ^c	$C_{16}Qu-PW$	25	Heterogeneous	Air	< 0.1	–
8	$C_{16}Qu-PW$	25	Heterogeneous	O_2	21.0	> 99
9	$C_{16}Qu-PW$	25	Heterogeneous	N_2	20.5	> 99
10	$C_{16}Qu-PW$	2.5	Heterogeneous	Air	14.8	> 99
11	$C_{16}Qu-PW$	2.5	Heterogeneous	N_2	4.7	> 99
12	$C_{16}Qu-PW$	2.5	Heterogeneous	O_2	15.2	> 99
13 ^b	$C_{16}Qu-Br$	7.5	Homogeneous	N_2	1.3	> 99
14 ^d	$C_{16}Qu-PW$	25	Heterogeneous	O_2	20.6	> 99
15 ^e	$C_{16}Qu-PW$	25	Heterogeneous	N_2	4.8	> 99
16 ^e	$C_{16}Qu-Br$	25	Homogeneous	N_2	< 0.1	–

^a Reaction conditions: benzene 1.28 mmol, acetonitrile 10 mL, water 1 mL, atmospheric air, RT, 10 h.

^b 75 μmol of $C_{16}Qu-Br$ was used to guarantee that equimolar quinine organic cations as that in 25 μmol of $C_{16}Qu-PW$ was charged into the reaction.

^c In dark.

^d A mixture of acetonitrile (10 mL) and D_2O (1 mL) was used as the solvent.

^e Acetonitrile (10 mL) was used as the solvent.

and higher photocurrent density (Fig. 4B) of former relative to those of latter, indicating that the present strategy not only reaches the heterogenization

of the organic salt but also improves the photocatalytic activity by inhibiting the recombination of photoexcited carriers to promote their generation, separation and transport. Moreover, inert activity of Na_3PW suggests that $C_{16}Qu^+$ cations mainly respond to the photocatalytic activity and pairing with PW^{3-} anions affords the heterogeneous catalyst with improved activity. Parallel test of other C_nQu-Br and C_nQu-PW samples (Table S2) demonstrated that the activity is closely related to the length of the carbon chain in the organic cations and C_nQu-PW always exhibited the higher yield than the corresponding C_nQu-Br precursor. The yield of phenol was 14.4% by using C_2Qu-PW and increased continuously with increasing carbon chain, reaching the maximum over $C_{16}Qu-PW$ (Entries 6–9). Owing to the solubility of $C_{2-18}Qu-Br$ and $C_{2-12}Qu-PW$ in the polar solvents, these samples are homogeneous catalysts under the present reaction conditions. The sample $C_{18}Qu-PW$ also has the heterogeneous nature and afforded similar activity (yield: 20.5%) to that of $C_{16}Qu-PW$ (Entry 10). These results suggest that the long carbon chain in the organic cations favors to construct high performing heterogeneous catalyst. After reaction, the catalyst $C_{16}Qu-PW$ was conveniently recovered by filtration. Photocatalytic recyclability was measured in a six-run test (Fig. 5A). $C_{16}Qu-PW$ displayed the stable recycling activity, suggestive of the remarkable reusability. Structural characterization of the recovered $C_{16}Qu-PW$ after 6th run indicated that the spent catalyst exhibited almost the same IR (Fig. S9) and UV-vis spectra (Fig. S10) as those of the fresh one. The result of elemental analysis over this spent $C_{16}Qu-PW$ (Table S1, Entry 11) is also identical to that of the fresh catalyst. These preserved structural characters are responsive to the well recycling performance.

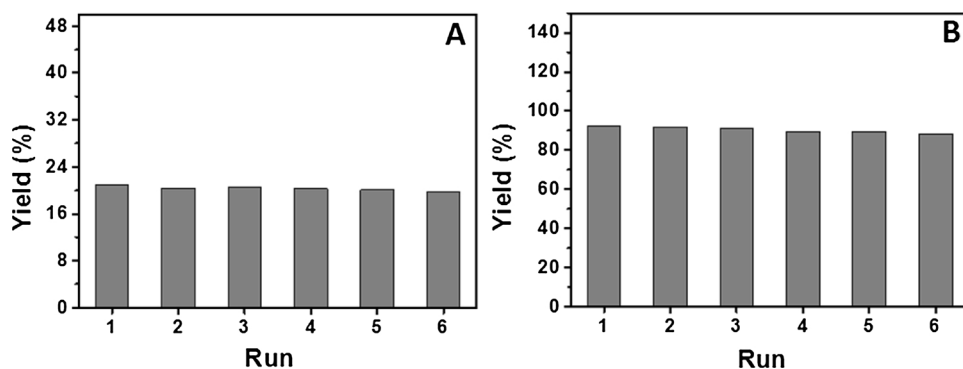


Fig. 5. Catalytic reusability of C₁₆Qu-PW in (A) the selective oxidation of benzene (Reaction conditions: benzene 1.28 mmol, acetonitrile 10 mL, water 1 mL, atmospheric air, RT, 10 h) and (B) the selective oxidation of benzyl alcohol (Reaction conditions: benzyl alcohol 0.1 mmol, acetonitrile 10 mL, atmospheric air, RT, 4 h).

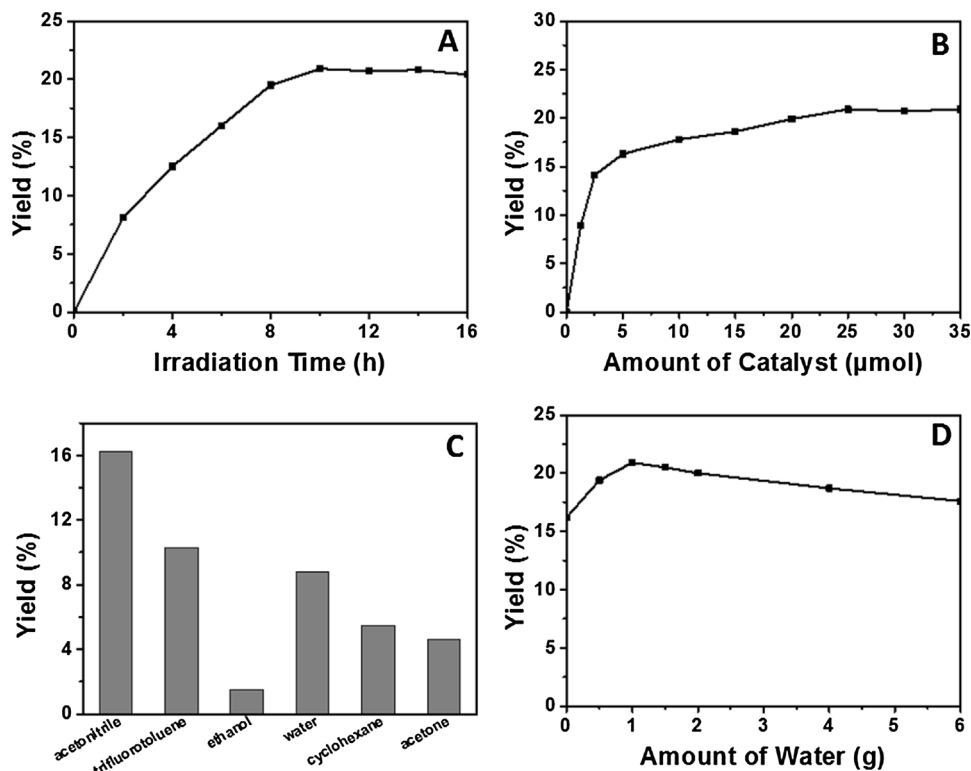


Fig. 6. Influences of reaction conditions on the photocatalytic hydroxylation of benzene to phenol by using C₁₆Qu-PW. (A) irradiation time, (B) amount of catalyst, (C) solvent type and (D) amount of water. Reaction conditions: benzene 1.28 mmol, solvent 10 mL, atmospheric air, RT. For each figure there is a specific parameter changed.

Activity of C₁₆Qu-PW under different reaction conditions was investigated by varying the reaction time, catalyst dosage and solvent. As is shown in Fig. 6A, the yield of phenol increased continuously with the reaction time, reaching the highest one at 10 h. Further increasing the time caused no obvious variation of the yield. Fig. 6B shows the influence of catalyst dosage. Gradually increasing the dosage ranging 0–5 μmol led to a rapid rise of phenol yield and excessive catalyst only slightly enhanced the activity. When the catalyst dosage was higher than 25 μmol, the phenol yield kept constant. Interestingly, no by-product was detectable at high catalyst dosage, visualizing the high selectivity. By fixing the reaction time at 10 h and catalyst dosage at 25 μmol, the solvent effect was explored (Fig. 6C). Among them, the yield of phenol by using acetonitrile was 16.2%, higher than those by using trifluorotoluene, ethanol, water, cyclohexane or acetone. Higher yield was found by using a mixture of acetonitrile and water that those by using a single solvent. The composition of this binary solvents significantly affected the activity and the presence of small amount of water afforded a high yield of 20.9%. There are two major reasons contributing to the higher yield of phenol by using a mixture of acetonitrile and water than those by using a single solvent. On the one hand, because benzene is soluble in organic acetonitrile but insoluble in water [61], biphasic reaction medium composed of suitable proportion

of acetonitrile and water provides better solubility of reactant benzene than water. On the other hand, water served as the intermediate O source in the reaction (Fig. S11, details seen below) [62], facilitating the O transfer, and thus a mixture of acetonitrile and water endows more intermediate O resource than that of acetonitrile. The catalyst dosage was explored in a wide range from 1.25 to 35 μmol (Fig. 6D). The phenol yield increased rapidly at the low catalyst dosage (1.25–5 μmol) and varied slightly at higher catalyst dosage (5–35 μmol). It was found that the maximum yield was observed with the catalyst dosage of 25 μmol. No obvious light scattering effect was observed [63]. Based on these results, the suitable catalyst dosage was fixed at 25 μmol (Fig. 6D).

C₁₆Qu-PW catalyzed photocatalytic hydroxylation of benzene to phenol was carried out under different conditions (Table 1). When 25 μmol catalyst was used, the yields were 21.0% and 20.5% under O₂ and N₂ atmosphere (Entries 8 and 9), respectively. These two values are close to that under air atmosphere. The same yield of phenol under O₂, air and N₂ atmosphere by using 25 μmol C₁₆Qu-PW is assigned to that the oxygen in the PW anions [64] and water [62] served as the intermediate oxygen sources that afforded sufficient oxygen atom to be transferred into phenol even under N₂ atmosphere when large dosage of catalyst was charged into the reaction. When the catalyst dosage of

$C_{16}Qu$ -PW was decreased to be 2.5 μmol , the phenol yields decreased to 15.2%, 14.8% and 4.7% under O_2 , air and N_2 atmosphere (Entries 10–12), respectively. The dramatically declined yield under N_2 atmosphere is attributed to the decreased intermediate oxygen source from the PW anions, the reduced state of which is not regenerated under N_2 atmosphere. D-isotope experiment was performed by using a mixture of acetonitrile and H_2O into D_2O (Fig. S11 and Table 1, Entry 14). The formation of partial CH_4DOH indicates the participation of water in the reaction [62]. $C_{16}Qu$ -PW (25 μmol) catalyzed reaction under N_2 atmosphere using acetonitrile as the solvent provided lower phenol yield of 4.8% than that (20.5%) using a mixture of acetonitrile and water (Table 1, Entry 15), additionally revealing the participation of water. In addition, under N_2 atmosphere, the phenol yield was 1.3% over $C_{16}Qu$ -Br without PW anions by using a mixture of acetonitrile (Table 1, Entry 13) and water and then declined to $< 0.1\%$ by using acetonitrile (Table 1, Entry 16). These results additionally validate the involvement of PW and water in the reaction as the intermediate oxygen source. Owing to this reason, similar phenol yield was observed by using the large dosage of $C_{16}Qu$ -PW. These results under N_2 atmosphere also suggest that the molecular dioxygen in air or O_2 atmosphere serves as the terminal oxygen source. On the basis of the observations described above, we deduce that photocatalytic hydroxylation of benzene to phenol involves multipaths. Oxygen in the PW anions was preferentially transferred into the phenol, and water also involved in the reaction to promote product formation.

To gain deep insight, the electronic state of $C_{16}Qu$ -PW during the reaction was monitored by in-situ ESR spectra, as is shown in Fig. 7A. Before illumination, no ESR signal was observed, suggestive of the high valent for the W^{6+} species in the original $C_{16}Qu$ -PW. A signal at 3650 G attributable to low-valent W^{5+} species emerged under irradiation and the intensity of this peak increased gradually with elongating the irradiation time. This phenomenon indicates that the initial W^{6+} species were gradually transformed into W^{5+} species during this photocatalytic reaction [65]. After N_2 -mediated reaction, the spent $C_{16}Qu$ -PW was recovered and the corresponding time-resolved UV-vis spectra were collected (Fig. 7B). Compared with the fresh catalyst, this spent one exhibited an additional absorption band ranging 600–850 nm that is assignable to the formation of heteropoly blue containing low-valenced W^{5+} species, in line with the result of in-situ ESR spectra [66]. The intensity of the above absorption band was rapidly attenuated to a low level in about 15 min when the spent catalyst was exposed in the air, indicating that the W^{5+} species were oxidized into W^{6+} species. These results also indicate that oxygen in the PW anions acts as the intermediate oxygen source and the one in the O_2 serves as the terminal oxygen source to regenerate the PW anions.

Based on the results above and previous researches [26,27], a possible mechanism is proposed in Fig. S12. Under irradiation, $C_{16}Qu^+$ absorbed photon and transformed into excited state of $C_{16}Qu^{+*}$, which reacted with benzene to form $C_{16}Qu^{\cdot}$ and benzene radical cation. The

interaction of benzene radical cation with water yields the OH-adduct radical. On the one hand, O_2 can be reduced by $C_{16}Qu^{\cdot}$ to $O_2^{\cdot-}$, protonation of which generates $HO_2^{\cdot-}$. Phenol could be produced through the hydrogen abstraction of $HO_2^{\cdot-}$ from the OH-adduct radical, associating with formation of H_2O_2 (Fig. S12, Part A) [26]. In the presence of PW anions (Fig. S12, Part B), intermolecular charge transfer from $C_{16}Qu^{\cdot}$ to PW anions caused the formation of PW^{\cdot} and regeneration of organic cation to be $C_{16}Qu^+$. The interaction of PW^{\cdot} with benzene could produce phenol and heteropoly blue species. This is responsive to the phenol formation under N_2 atmosphere when the reaction was catalyzed by $C_{16}Qu$ -PW even under water-free condition (Table 1, Entry 15). Additional oxidation of W^{5+} species in the heteropoly blue regenerated the PW anions. It means that the phenol formation catalyzed by $C_{16}Qu$ -PW may undergo multi-pathways, in line with the higher activity of this catalyst by using a mixture of acetonitrile and water than that by using acetonitrile. Though the details are still to be explored, the present results show that PW anions promote generation, separation and transport of the photoinduced carriers and thus $C_{16}Qu$ -PW exhibited higher activity than $C_{16}Qu$ -Br [67,68].

3.3. Photocatalytic selective oxidation of benzyl alcohol

Aromatic aldehydes are important industrial raw materials of fine chemicals and have been widely applied in the fields of medicine, dyes, perfumes and pesticides [69]. Among them, benzaldehyde is the simplest aromatic aldehyde with an active carbonyl group and traditionally produced through the oxidation of toluene or the hydrolysis of benzyl chloride, associating with hazardous or corrosive reagents and low selectivity inevitably [70]. Photocatalytic oxidation of benzyl alcohol with easily available oxidant O_2 is among the most promising atom efficient and environmental way to synthesize benzaldehyde under mild conditions. Although many photocatalysts, such as TiO_2 , $BiOCl$, $g-C_3N_4$ and CdS , have been investigated in this selective oxidation reaction [71], the design of highly efficient heterogeneous catalysts is still one urgent affair. In this study, the catalyst $C_{16}Qu$ -PW was further applied in the photocatalytic oxidation of benzyl alcohol to benzaldehyde with excellent activity and selectivity. Urgent affair is developing more efficient photocatalysts to improve product selectivity. In this study, the catalyst $C_{16}Qu$ -PW was further applied in the photocatalytic oxidation of benzyl alcohol to benzaldehyde with excellent activity and selectivity. Parallel test was also performed on other control samples. As listed in Table 2, the yield of benzaldehyde was low by using Qu , $C_{16}Br$ or Na_3PW as the homogeneous photocatalysts (Entries 1–3). $C_{16}Qu$ -Br afforded a yield of 82.5% and $C_{16}Qu$ -PW offered a higher yield of 92.4% (Entries 4 and 5). By contrast, no benzaldehyde was produced under a catalyst-free or irradiation-free condition (Entries 6 and 7). $C_{16}Qu$ -PW served as a heterogeneous catalyst in this reaction mediate and exhibited stable reusability in a 6-run recycling test (Fig. 5B). C_nQu -Br and C_nQu -PW samples were tested (Table S3) and the

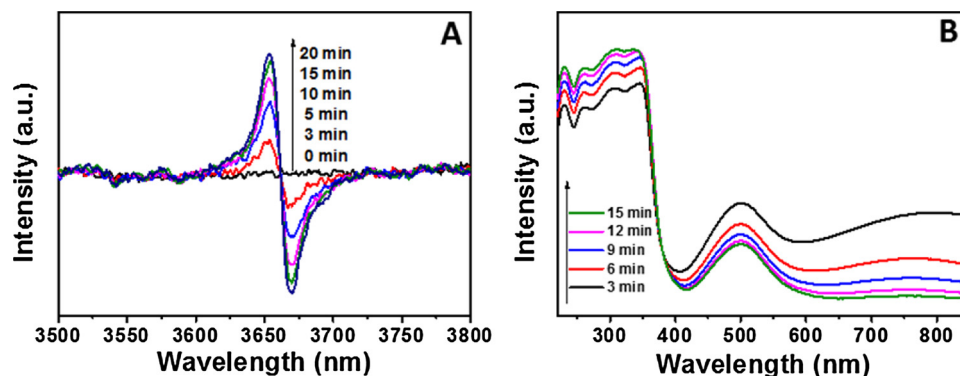
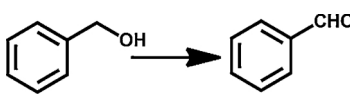


Fig. 7. (A) In-situ ESR spectra of $C_{16}Qu$ -PW in reaction system (containing benzene 1.28 mmol, acetonitrile 10 mL, water 1 mL) and (B) UV-vis spectra of recovered $C_{16}Qu$ -PW with different exposure time in the air.

Table 2
Photocatalytic selective oxidation of benzyl alcohol to benzaldehyde^a.



Entry	Catalyst	Catalyst dosage (μmol)	Phenomenon	Yield (%)	Sel. (%)
1	Qu	7.5	Homogeneous	3.4	92.3
2	C ₁₆ Br	7.5	Homogeneous	< 0.1	–
3	Na ₃ PW	2.5	Homogeneous	< 0.1	–
4	C ₁₆ Qu-Br	7.5	Homogeneous	82.5	98.6
5	C ₁₆ Qu-PW	2.5	Heterogeneous	92.4	97.4
6 ^b	C ₁₆ Qu-PW	2.5	Heterogeneous	< 0.1	–
7	None	–	–	< 0.1	–

^a Reaction conditions: benzyl alcohol 0.1 mmol, acetonitrile 10 mL, atmospheric air, RT, 4 h.

^b In dark.

formers were homogeneous catalysts with slightly inferior activity than that of the latter ones. The solvent and reaction time of C₁₆Qu-Br catalyzed reaction were also explored in the photocatalytic oxidation of benzyl alcohol to benzaldehyde. Excessive reaction time caused the decline of the yield due to the over-oxidation of benzaldehyde (Fig. S13). Acetonitrile was found to be the best solvent for this reaction while a mixture of acetonitrile and water offered a slightly inferior phenol yield (Table S4, Entry 1). The reason may be assigned to that water was not involved in the oxidation of benzyl alcohol [72,73].

4. Conclusion

In summary, IL-POM hybrids composed of quinoline cations and phosphotungstic (PW) anions were constructed as the efficient recyclable heterogeneous photocatalysts by modulating the carbon chain in the organic cations. They exhibited the high yield and stable reusability in the benzene hydroxylation to phenol and oxidation of benzyl alcohol to benzaldehyde, in which the atmospheric air was used as the sole terminal oxidant. The strong ionic interaction between the organic cations and inorganic anions led to the heterogeneous nature of this photocatalysis. The unique redox property of the POM anions benefits to inhibit the recombination of photo-induced carriers and thus the activity of heterogeneous IL-POM hybrid is superior to the homogeneous quinoline salt precursor. This present strategy provides an effective and versatile route towards highly efficient heterogeneous photocatalyst.

Acknowledgements

This work was supported by the National Natural Science Foundation of China (Nos. U1662107, 21476109, 21136005 and 21303084) and the Project of Priority Academic Program Development of Jiangsu Higher Education Institutions (PAPD).

Appendix A. Supplementary data

Supplementary material related to this article can be found, in the online version, at doi:<https://doi.org/10.1016/j.mcat.2019.110397>.

References

- H. Xu, X. Liu, C. Cao, B. Zhao, P. Cheng, L. He, A porous metal-organic framework assembled by [Cu₃₀] nanocages: serving as recyclable catalysts for CO₂ fixation with aziridines, *Adv. Sci.* 3 (2016) 1600048–1600054.
- M.J. Climent, A. Corma, S. Iborra, Heterogeneous catalysts for the one-pot synthesis of chemicals and fine chemicals, *Chem. Rev.* 111 (2011) 1072–1133.
- R.A. Sheldon, Fundamentals of green chemistry: efficiency in reaction design, *Chem. Soc. Rev.* 41 (2012) 1437–1451.
- H.U. Blaser, M. Studer, The role of catalysis for the clean production of fine chemicals, *Appl. Catal. A Gen.* 189 (1999) 191–204.
- Y. Morimoto, S. Bunno, N. Fujieda, H. Sugimoto, S. Itoh, Direct hydroxylation of benzene to phenol using hydrogen peroxide catalyzed by nickel complexes supported by pyridylalkylamine ligands, *J. Am. Chem. Soc.* 137 (2015) 5867–5870.
- S. Verma, R.B.N. Baig, M.N. Nadagouda, R.S. Varma, Hydroxylation of benzene via C–H activation using bimetallic CuAg@g-C₃N₄, *ACS Sustain. Chem. Eng.* 5 (2017) 3637–3640.
- H. Wang, C. Wang, M. Zhao, Y. Yang, L. Fang, Y. Wang, H₅PMo₁₀V₂O₄₀ anchor by –OH of the Titania nanotubes: highly efficient heterogeneous catalyst for the direct hydroxylation of benzene, *Chem. Eng. Sci.* 177 (2018) 399–409.
- G.I. Panov, *Advances in oxidation catalysis; oxidation of benzene to phenol by nitrous oxide*, *Cattech* 4 (2000) 18–31.
- S. Niwa, M. Eswaramoorthy, J. Nair, A. Raj, N. Ito, H. Shoji, T. Namba, F. Mizukami, A one-step conversion of benzene to phenol with a palladium membrane, *Science* 305 (2002) 105–107.
- Yamada M, K.D. Karlin, S. Fukuzumi, One-step selective hydroxylation of benzene to phenol with hydrogen peroxide catalysed by copper complexes incorporated into mesoporous silica-alumina, *Chem. Sci.* 7 (2016) 2856–2863.
- K. Hirose, K. Ohkubo, S. Fukuzumi, Catalytic hydroxylation of benzene to phenol by dioxygen with an NADH analogue, *Chem. Eur. J.* 22 (2016) 12901–12909.
- T. Tsuji, A.A. Zaoputra, Y. Hitomi, K. Mieda, Ti Ogura, Y. Shiota, K. Yoshizawa, H. Sato, M. Kodera, Specific enhancement of catalytic activity by a dicopper core: selective hydroxylation of benzene to phenol with hydrogen peroxide, *Angew. Chem. Int. Ed.* 56 (2017) 7779–7782.
- Yamada M, K.D. Karlin, S. Fukuzumi, One-step selective hydroxylation of benzene to phenol with hydrogen peroxide catalysed by copper complexes incorporated into mesoporous silica-alumina, *Chem. Sci.* 7 (2016) 2856–2863.
- D. Bianchi, R. Bortolo, R. Tassinari, M. Marco, V. Rodolfo, A novel iron-based catalyst for the biphasic oxidation of benzene to phenol with hydrogen peroxide, *Angew. Chem. Int. Ed.* 39 (2000) 4321–4323.
- Z. Long, G. Chen, S. Liu, F. Huang, L. Sun, Z. Qin, Q. Wang, Y. Zhou, J. Wang, Synergistic combination of graphitic C₃N₄ and polyoxometalate-based phase-transfer catalyst for highly efficient reductant-free aerobic hydroxylation of benzene, *Chem. Eng. J.* 334 (2018) 873–881.
- Y. Zhou, Z. Ma, J. Tang, N. Yan, Y. Du, S. Xi, K. Wang, W. Zhang, Ha. Wen, J. Wang, Immediate hydroxylation of arenes to phenols via V-containing all-silica ZSM-22 zeolite triggered non-radical mechanism, *Nat. Commun.* 9 (2018) 2931–2940.
- Y. Ide, N. Nakamura, H. Hattori, R. Ogino, M. Ogawa, M. Sadakane, T. Sano, Sunlight-induced efficient and selective photocatalytic benzene oxidation on TiO₂-supported gold nanoparticles under CO₂ atmosphere, *Chem. Commun. (Camb.)* 41 (2011) 11531–11533.
- M. Oelgemöller, Solar photochemical synthesis: from the beginnings of organic photochemistry to the solar manufacturing of commodity chemicals, *Chem. Rev.* 116 (2016) 9664–9682.
- X. Lang, X. Chen, J. Zhao, Heterogeneous visible light photocatalysis for selective organic transformations, *Chem. Soc. Rev.* 43 (2014) 473–486.
- S. Fukuzumi, K. Ohkubo, One-step selective hydroxylation of benzene to phenol, *Asian J. Org. Chem.* 4 (2015) 836–845.
- S. Fukuzumi, K. Ohkubo, Organic synthetic transformations using organic dyes as photoredox catalysts, *Org. Biomol. Chem.* 12 (2014) 6059–6071.
- L. Chen, J. Tang, L.-N. Song, P. Chen, J. He, C.-T. Au, S.-F. Yin, Heterogeneous photocatalysis for selective oxidation of alcohols and hydrocarbons, *Appl. Catal. B: Environ.* 242 (2019) 379–388.
- O. Tomita, B. Ohtani, R. Abe, Highly selective phenol production from benzene on a platinum-loaded tungsten oxide photocatalyst with water and molecular oxygen: selective oxidation of water by holes for generating hydroxyl radical as the predominant source of the hydroxyl group, *Catal. Sci. Technol.* 4 (2014) 3850–3860.
- Z. Zheng, B. Huang, X. Qin, X. Zhang, Y. Dai, M.-H. Whangbo, Facile in situ synthesis of visible-light plasmonic photocatalysts M@TiO₂ (M ¼ Au, Pt, Ag) and evaluation of their photocatalytic oxidation of benzene to phenol, *J. Mater. Chem.* 21 (2011) 9079–9087.
- Y. Ide, M. Matsuoka, M. Ogawa, Efficient visible-light-induced photocatalytic activity on gold-nanoparticle-supported layered titanate, *J. Am. Chem. Soc.* 132 (2010) 16762–16764.
- K. Ohkubo, T. Kobayashi, S. Fukuzumi, Direct oxygenation of benzene to phenol using quinolinium ions as homogeneous photocatalysts, *Angew. Chem. Int. Ed.* 50 (2011) 8652–8655.
- D.A. Kalashnikov, A.V. Paterova, S.P. Kulik, L.A. Krivitsky, Infrared spectroscopy with visible light, *Nat. Photonics* 10 (2016) 98–101.
- P. Chen, L. Chen, Y. Zeng, F. Ding, X. Jiang, N. Liu, C.-T. Au, S.-F. Yin, Three-dimensional hierarchical heterostructure of CdWO₄ microrods decorated with Bi₂WO₆ nanoplates for high-selectivity photocatalytic benzene hydroxylation to phenol, *Appl. Catal. B: Environ.* 234 (2018) 311–317.
- D. Ravelli, M. Fagnoni, A. Albini, Photoorganocatalysis. What for? *Chem. Soc. Rev.* 42 (2013) 97–113.
- L. Liu, L. Zhou, D. Jiang, Y. Gu, Multicomponent reactions of Aldo-X bifunctional reagent α-oxo ketene dithioacetals and indoles or amines: divergent synthesis of dihydrocoumarins, quinolines, furans, and pyrroles, *Asian J. Org. Chem.* 5 (2016) 367–372.
- M. Zhang, C. Chen, W. Ma, J. Zhao, Visible-light-induced aerobic oxidation of alcohols in a coupled photocatalytic system of dye-sensitized TiO₂ and TEMPO, *Angew. Chem. Int. Ed.* 47 (2008) 9730–9733.
- A. Karakulina, A. Gopakumar, İ. Akçok, B.L. Roulier, T.L. Grange, S.A. Katsyuba, S. Das, P.J. Dyson, A rhodium nanoparticle-lewis acidic ionic liquid catalyst for the chemoselective reduction of heteroarenes, *Angew. Chem. Int. Ed.* 128 (2016)

- 300–304.
- [33] M. Paszkiewicz, J. Łuczak, W. Lisowski, P. Paty, A. Zaleska-Medynska, The ILs-assisted solvothermal synthesis of TiO₂ spheres: the effect of ionic liquids on morphology and photoactivity of TiO₂, *Appl. Catal. B: Environ.* 184 (2016) 223–237.
- [34] S.-g. Lee, Functionalized imidazolium salts for task-specific ionic liquids and their applications, *Chem. Commun. (Camb.)* 10 (2006) 1049–1063.
- [35] Y. Zhou, G. Chen, Z. Long, J. Wang, Recent advances in polyoxometalate-based heterogeneous catalytic materials for liquid-phase organic transformations, *RSC Adv.* 4 (2014) 42092–42113.
- [36] Y. Leng, J. Wang, D. Zhu, X. Ren, H. Ge, L. Shen, Heteropolyanion-based ionic liquids: reaction-induced self-separation catalysts for esterification, *Angew. Chem. Int. Ed.* 48 (2009) 168–171.
- [37] L. Yu, Y. Ding, M. Zheng, H. Chen, J. Zhao, [β -SiNi₂W₁₀O₃₆(OH)₂(H₂O)₄]²⁴⁻: a new robust visible light-driven water oxidation catalyst based on nickel-containing polyoxometalate, *Chem. Commun. (Camb.)* 52 (2016) 14494–14497.
- [38] E. Rafiee, F. Mirnezami, Keggin-structured polyoxometalate-based ionic liquid salts: thermoregulated catalysts for rapid oxidation of sulfur-based compounds using H₂O₂ and extractive oxidation desulfurization of sulfur-containing model oil, *J. Mol. Liq.* 199 (2014) 156–161.
- [39] C. Chen, H. Yuan, H. Wang, Y. Yao, W. Ma, J. Chen, Z. Hou, Highly efficient epoxidation of allylic alcohols with hydrogen peroxide catalyzed by peroxoniobate-based ionic liquids, *ACS Catal.* 6 (2016) 3354–3364.
- [40] P. Zhao, M. Zhang, Y. Wu, J. Wang, Heterogeneous selective oxidation of sulfides with H₂O₂ catalyzed by ionic liquid-based polyoxometalate salts, *Ind. Eng. Chem. Res.* 51 (2012) 6641–6647.
- [41] C. Streb, New trends in polyoxometalate photoredox chemistry: From photosensitisation to water oxidation catalysis, *Dalton Trans.* 41 (2012) 1651–1659.
- [42] M. Misono, Heterogeneous catalysis by heteropoly compounds of molybdenum and tungsten, *Catal. Rev. Sci. Eng.* 29 (1987) 269–321.
- [43] A.A. Alshaheri, M.I.M. Tahir, M.B.A. Rahman, Catalytic oxidation of cyclohexane using transition metal complexes of dithiocarbamate Schiff base, *Chem. Eng. J.* 327 (2017) 423–430.
- [44] X. Yan, P. Zhu, J. Fei, J. Li, Self-assembly of peptide-inorganic hybrid spheres for adaptive encapsulation of guests, *Adv. Mater.* 22 (2010) 1283–1287.
- [45] T.A. Saleh, M.M. Al-Shalalfeh, A.A. Al-Saadi, Graphene Dendrimer-stabilized silver nanoparticles for detection of methimazole using Surface-enhanced Raman scattering with computational assignment, *Sci. Rep.* 6 (2016) 32185.
- [46] T. Rajkumar, G.R. Rao, Investigation of hybrid molecular material prepared by ionic liquid and polyoxometalate anion, *J. Chem. Sci. Bangalore (Bangalore)* 120 (2008) 587–594.
- [47] S.S. Sakate, S.B. Kamble, R.C. Chikate, C.V. Rode, MCM-41-supported phosphotungstic acid-catalyzed cleavage of C–O bond in allyl aryl ethers, *New J. Chem.* 41 (2017) 4943–4949.
- [48] H. Wang, G. Wang, Z. Liu, Z. Jin, Strategy of nitrogen defects sponge from g-C₃N₄ nanosheets and Ni-Bi-Se complex modification for efficient dye-sensitized photocatalytic H₂ evolution, *Mole. Catal.* 453 (2018) 1–11.
- [49] M.B. Abdelaziz, B. Chouchene, L. Balan, T. Gries, G. Medjahdi, H. Ezzaouia, R. Schneider, One pot synthesis of bismuth oxide/graphitic carbon nitride composites with high photocatalytic activity, *Mole. Catal.* 463 (2019) 110–118.
- [50] Z. Guo, Q. Jiang, Y. Shi, J. Li, X. Yang, W. Hou, Y. Zhou, J. Wang, Tethering dual hydroxyls into mesoporous poly (ionic liquid)s for chemical fixation of CO₂ at ambient conditions: a combined experimental and theoretical study, *ACS Catal.* 10 (2017) 6770–6780.
- [51] R. He, X. Huang, P. Zhao, B. Han, T. Wu, Y. Wu, The synthesis of 5-hydroxymethylfurfural from glucose in biphasic system by phosphotungstic acidified titanium-zirconium dioxide, *Waste Biomass Valor.* 4 (2018) 657–668.
- [52] T. Rajkumar, G.R. Rao, Characterization of hybrid molecular material prepared by 1-butyl 3-methyl imidazolium bromide and phosphotungstic acid, *Mater. Lett.* 62 (2008) 4134–4136.
- [53] S. Aloïse, C. Ruckebusch, L. Blanchet, J. Réhault, G. Buntinx, J.P. Huvenne, The benzophenone S₁(n, π*)→T₁(n, π*) states intersystem crossing reinvestigated by ultrafast absorption spectroscopy and multivariate curve resolution, *J. Phys. Chem. A* 112 (2008) 224–231.
- [54] T. Peppel, M. Köckerling, Investigations on a series of ionic liquids containing the [CollBr₃quin]⁻ Anion(quin = quinoline), *Cryst. Growth Des.* 11 (2011) 5461–5468.
- [55] T. Peppel, A. Hinz, M. Köckerling, Salts with the [NiBr₃(L)]⁻ complex anion (L = 1-methylimidazole, 1-methylbenzimidazole, quinoline, and triphenylphosphane) and low melting points: a comparative study, *Polyhedron* 52 (2013) 482–490.
- [56] S. Meng, X. Ye, X. Ning, M. Xie, X. Fu, S. Chen, Selective oxidation of aromatic alcohols to aromatic aldehydes by BN/metal sulfide with enhanced photocatalytic activity, *Appl. Catal. B: Environ.* 182 (2016) 356–368.
- [57] M. Yang, Y. Xu, Selective photoredox using graphene-based composite photocatalysts, *Phys. Chem. Chem. Phys.* 15 (2013) 19102–19118.
- [58] Y. Zhang, Z. Jin, Y. Su, G. Wang, Charge separation and electron transfer routes modulated with Co–Mo–P over g-C₃N₄ photocatalyst, *Mole. Catal.* 462 (2019) 46–55.
- [59] N. Zhang, M. Yang, Z. Tang, Y. Xu, Toward improving the graphene–semiconductor composite photoactivity via the addition of metal ions as generic interfacial mediator, *ACS Nano* 8 (2013) 623–633.
- [60] N. Zhang, M. Yang, S. Liu, Y. Sun, Y. Xu, Waltzing with the versatile platform of graphene to synthesize composite photocatalysts, *Chem. Rev.* 115 (2015) 10307–10377.
- [61] D. Wang, M. Wang, Z. Li, Fe-based metal–organic frameworks for highly selective photocatalytic benzene hydroxylation to phenol, *ACS Catal.* 5 (2015) 6852–6857.
- [62] H. Yuzawa, M. Aoki, K. Otake, T. Hattori, H. Itoh, H. Yoshida, Reaction mechanism of aromatic ring hydroxylation by water over platinum-loaded titanium oxide photocatalyst, *J. Phys. Chem. C* 116 (2012) 25376–25387.
- [63] J. Ran, T. Ma, G. Gao, X. Du, S. Qiao, Porous P-doped graphitic carbon nitride nanosheets for synergistically enhanced visible-light photocatalytic H₂ production, *Energy Environ. Sci.* 8 (2015) 3708–3717.
- [64] H. Park, W. Choi, Photocatalytic conversion of benzene to phenol using modified TiO₂ and polyoxometalates, *Catal. Today* 101 (2005) 291–297.
- [65] Y. Leng, J. Wang, D. Zhu, M. Zhang, P. Zhao, Z. Long, J. Huang, Polyoxometalate-based amino-functionalized ionic solid catalysts lead to highly efficient heterogeneous epoxidation of alkenes with H₂O₂, *Green Chem.* 13 (2011) 1636–1639.
- [66] G. Chen, Y. Zhou, Z. Long, X. Wang, J. Li, J. Wang, Mesoporous polyoxometalate-based ionic hybrid as a triphasic catalyst for oxidation of benzyl alcohol with H₂O₂ on water, *ACS Appl. Mater. Interfaces* 6 (2014) 4438–4446.
- [67] R. Liang, R. Chen, F. Jing, N. Qin, L. Wu, Multifunctional polyoxometalates encapsulated in MIL-100(Fe): highly efficient photocatalysts for selective transformation under visible light, *Dalton Trans.* 44 (2015) 18227–18236.
- [68] J. Liao, H. Zhang, S. Wang, J. Yong, X. Wu, R. Yu, C. Lu, Multifunctional radical-doped polyoxometalate-based host–guest material: photochromism and photocatalytic activity, *Inorg. Chem.* 54 (2015) 4345–4350.
- [69] H. She, H. Zhou, L. Li, L. Wang, J. Huang, Q. Wang, Nickel-doped excess oxygen defect titanium dioxide for efficient selective photocatalytic oxidation of Benzyl alcohol, *ACS Sustain. Chem. Eng.* 6 (2018) 11939–11948.
- [70] C. Li, G. Xu, B. Zhang, J. Gong, High selectivity in visible-light-driven partial photocatalytic oxidation of benzyl alcohol into benzaldehyde over single-crystalline rutile TiO₂ nanorods, *Appl. Catal. B: Environ.* 115 (2012) 201–208.
- [71] L. Chen, J. Tang, L. Song, P. Chen, C.T.Au J He, S. Yin, Heterogeneous photocatalysis for selective oxidation of alcohols and hydrocarbons, *Appl. Catal. B: Environ.* 242 (2019) 379–388.
- [72] D. Tsukamoto, Y. Shiraishi, Y. Sugano, S. Ichikawa, S. Tanaka, T. Hirai, Gold nanoparticles located at the interface of anatase/rutile TiO₂ particles as active plasmonic photocatalysts for aerobic oxidation, *J. Am. Chem. Soc.* 134 (2012) 6309–6315.
- [73] S. Yurdakal, G. Palmisano, V. Loddo, O. Alagöz, V. Augugliaro, L. Palmisano, Selective photocatalytic oxidation of 4-substituted aromatic alcohols in water with rutile TiO₂ prepared at room temperature, *Green Chem.* 11 (2009) 510–516.